Journal of Environmental Chemical Engineering 11 (2023) 109139

Contents lists available at ScienceDirect

Journal of Environmental Chemical Engineering

journal homepage: www.elsevier.com/locate/jece

Voltammetric and electrodeposition study for the recovery of antimony from effluents generated in the copper electrorefining process

L. Hernández-Pérez, J. Carrillo-Abad, E.M. Ortega, V. Pérez-Herranz, M.T. Montañés, M. C. Martí-Calatayud *

IEC Group, ISIRYM, Universitat Politècnica de València, Camí de Vera s/n, 46022, València P.O. Box 22012, E-46071, Spain

ARTICLE INFO

Editor: Apostolos Giannis

Keywords:
Industrial effluents
Antimony
Cyclic voltammetry
Electrodeposition
Hydrogen evolution reaction (HER)

ABSTRACT

Antimony is a metalloid with limited availability as a primary resource, but it is commonly found as an impurity in effluents generated in the copper metallurgy. Thus, the development of clean and selective processes to recover antimony from these wastewaters would improve the sustainability of the copper production. In this work, an emulated effluent of the copper electrorefining industry that contains antimony and hydrochloric acid was characterized by means of voltammetric and electrodeposition tests using two different cell configurations: a static cell, and a dynamic cell with a rotating disk electrode (RDE). Voltammograms were obtained at varying hydrochloric acid and antimony concentrations, inversion potentials, scan rates and RDE rotation rates. Two main conclusions were drawn: (a) the deposition of antimony is a mass transfer-controlled process; and (b) an increase in hydrochloric acid concentration improves the deposition of antimony. The diffusion coefficient of antimony species was obtained applying the Randles-Ševčík and the Levich equations; both of them providing very similar values ($5.29 \pm 0.20 \cdot 10^{-6}$ cm^2 s^{-1}). The effective electrodeposition of antimony from highly concentrated hydrochloric acid solutions was demonstrated. The surface examination of the electrodes revealed that compact and adherent deposits of antimony could be obtained under operating conditions that minimize the hydrogen evolution reaction in both potentiostatic and galvanostatic modes. Intensified convective regimes by using the RDE improve the supply of dissolved antimony towards the electrode surface, thus leading to a notorious increase in current density and, consequently, in the rate of antimony deposition.

1. Introduction

Antimony was declared as a critical raw material by the European Union in 2011 due to the increasing supply-risk and economic relevance of this element [1]. Antimony compounds find a wide variety of applications; among them, as flame retardants, pigments, as components in diodes and electronics, and in batteries [2]. In the last years, the necessity of obtaining Sb from secondary sources has been highlighted on account of the shortage of antimony in natural sources [3]. Dupont et al. [4] reviewed several options to recover antimony from end-of-life products and industrial wastes. Antimony can be recovered from wastes generated during the processing of copper [5] and lead [6] among others. Leaching and adsorption techniques predominate in those studies. Navarro and Alguacil [5] studied the application of carbon adsorption for the recovery of antimony and arsenic from a copper electrorefining solution. Cao et al. [6] combined leaching and distillation to obtain $SbCl_3$ from lead anode slime. In some works, leaching is also combined with electrodeposition to obtain metallic Sb: Ubaldini et al. [7] recovered metallic antimony from stibnite in a two-step process consisting of mineral leaching and antimony electrowinning. Bergmann and Koparal [8] studied the removal of antimony present in spent acid accumulators by electrodeposition. Koparal et al. [9] also investigated the viability of removing antimony from sulfuric acid solutions by electrodeposition.

The extraction of copper from mines and subsequent electrorefining is one of the industrial processes where the presence of Sb as a secondary material is more remarkable. Normally, antimony is present in copper ores in the form of impurities [4], which cause problems during the electrorefining process as they affect the quality of the final product. Moreover, the effluents generated during the process require from treatments in order to be properly discharged or reused.

Depending on the origin of the ores, copper is usually extracted by

* Corresponding author.
E-mail address: mcmarti@iqn.upv.es (M.C. Martí-Calatayud).

https://doi.org/10.1016/j.jece.2022.109139
Received 28 September 2022; Received in revised form 28 November 2022; Accepted 10 December 2022
Available online 10 December 2022

means of two different procedures: the hydrometallurgical method is employed with copper oxide and mixed minerals, while the pyrometallurgical method is used with copper sulfide ores [10]. In the hydrometallurgical process, leaching of the ores with sulfuric acid is followed by solvent extraction; where a solution concentrated in copper is finally obtained for the electrowinning process. In the pyrometallurgical process, grinding and milling of copper minerals is followed by subsequent steps of flotation, filtering and smelting. In both methods, after extraction of the metal, an electrorefining step is conducted to achieve copper of high purity (Fig. 1). As reviewed by Barros et al. [11], in some copper industries, the spent electrorefining electrolyte is passed through ion exchange beds to separate the metallic impurities and recycle the sulfuric acid employed in the electrorefining. In those industries, after a given number of cycles, the ion exchange system is regenerated with hydrochloric acid (HCl) and, as a result, a highly concentrated HCl solution containing mainly Sb and Bi, is obtained. Nowadays, this effluent is discarded without recovering the hydrochloric acid and the valuable metals present in it. As shown in the last steps of the scheme of Fig. 1, in this work, electrodeposition is proposed to treat the solution containing Sb to separate the metallic antimony from hydrochloric acid.

In order to implement the principles of circular economy in the copper production, Sb losses should be avoided and the recovered HCl solution should be further reused in the regeneration of ion exchange resins, thus ensuring a minimal release of effluents. Electrodeposition is a simple and economic technique that could be applied in the copper industry for recovering Sb and recycling HCl, as proposed by Thanu and Jayakumar [12]. One of the characteristic features of the electrolyte under study is the high concentration of HCl, 6 M, which causes corrosion and implies a challenge for the application of electrochemical techniques. On the contrary, the concentration of antimony present in the electrolyte is very low, of the order of millimoles per liter. Although there are some studies about antimony electrodeposition in hydrochloric acid, many of them investigated HCl concentrations below 1 M; for example, in the work carried out by Ward and Stickney [13], Sb was electrodeposited in a 1 mM HCl solution. Cao et al. [14] compared the effect of the HCl concentration (2, 3 and 4 M) on the electrodeposition of As-Sb alloys, obtaining the best results with the highest concentration of 4 M HCl.

The aim of the present research is to evaluate the electrodeposition of Sb present in an electrolyte with high hydrochloric acid concentrations. First, the electrochemical behavior of Sb-containing solutions was investigated by cyclic and linear sweep voltammetry. Afterwards, electrodeposition experiments were conducted in potentiostatic and galvanostatic mode. Finally, the deposits obtained were analyzed by scanning electron microscopy (SEM) and energy dispersive X-ray (EDX) measurements.

2. Materials and methods

2.1. Reagents and solutions

Synthetic solutions were prepared with analytical grade reagents, antimony (III) oxide (Sb_2O_3 99 %, Sigma-Aldrich) and HCl (37 %, Panreac), and distilled water with a maximum conductivity of 0.001 mS cm^{-1} (Type 2 water quality according to ASTM D1193-06 standard). Different concentrations of Sb (2–20 mM) and HCl (1.5 and 6 M), which are in the range measured in the real effluents [11], were used. The volume of electrolyte was 50 ml in all tests, which was replaced with new solution after each experiment.

2.2. Voltammetric study

Cyclic voltammetric experiments were conducted using an in-house designed three electrode cell with a special face-up electrode configuration that facilitates the removal of gas bubbles generated during the tests. The cell has been described in previous works [15] and will be referred to as the static cell. The working electrode was a platinum electrode (Metrohm for Autolab RDE) with an area of 0.071 cm^2. An Ag/AgCl (3 M KCl) electrode (Type 6.0733.100, Metrohm) and a platinum ring with an area of 1 cm^2 (Type Pt 805-S8/120, Mettler-Toledo) were employed as reference and counter electrodes, respectively. Cyclic voltammetric experiments were performed using a potential range from -1 to $+1$ $V_{Ag/AgCl}$ starting at the open circuit potential (OCP) toward negative potentials and using scan rates from 10 to 100 mV s^{-1}. In these tests, the concentrations of Sb and HCl were also varied to investigate the processes associated with each species present in the solutions. Several cycles were performed to stabilize the system and ensure the registration of reproducible results.

In order to study the effect of mass transfer on the electroreduction of antimony ions, cathodic polarization curves were performed using a

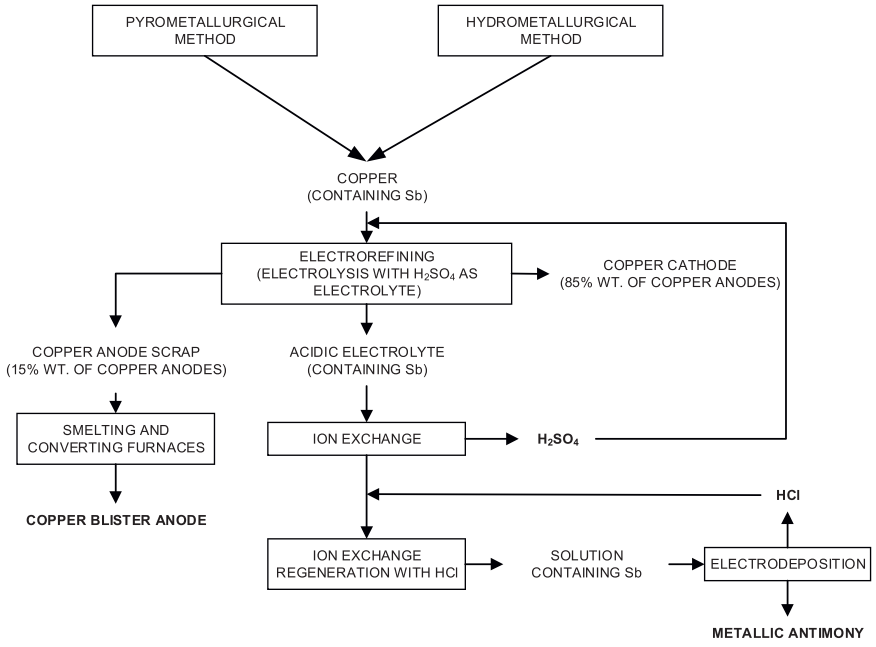

Fig. 1. Process flowsheet of the copper electrorefining including the subsequent steps for the recovery of metallic Sb.

conventional three electrode cell with a rotating disk electrode (RDE, Autolab RDE-2 Metrohm). The working electrodes were the platinum disk mentioned previously and a copper disk enclosed in Teflon with an area of 0.8 cm^2. The reference electrode was an Ag/AgCl (3 M KCl) electrode, and the counter electrode was the platinum ring indicated above. The experiments were executed at a scan rate of 10 mV s^{-1} and rotation rates ranging between 500 and 4500 rpm.

All electrochemical tests were carried out at room temperature (25 °C) using a potentiostat/galvanostat (Autolab PGSTAT 302N) and NOVA 1.10 software. Before each test, the working electrodes were polished with different grades of emery papers (500 and 4000 Grit), rinsed with distilled water and ethanol, and dried with air.

2.3. Electrodeposition experiments

The electrodeposition tests were conducted for 30 min using a 6 M HCl solution with a concentration of Sb of 2 mM, in potentiostatic and galvanostatic mode, and using both cells to show the influence of the rotation rate on the obtained Sb deposits. The working electrode was a copper disk enclosed in Teflon with an area of 0.8 cm^2. The potentials applied in the potentiostatic experiments were selected based on the voltammograms obtained previously. The current densities applied in the galvanostatic tests using the static cell were selected from the average values measured during the potentiostatic experiments. The electrodeposition experiments carried out with stirring were conducted at 1500 rpm.

Scanning electron microscopy (SEM, ZEISS Ultra 55) applying an acceleration voltage of 20 kV was used to examine the surface morphology of the Sb deposits. The composition of the deposits was evaluated by an energy dispersive X-ray analyzer (EDX) attached to the SEM.

3. Results and discussion

3.1. Electrochemical study using the static cell

Fig. 2 shows three consecutive cyclic voltammograms conducted to study the deposition of Sb(III) over a Pt electrode in the potential range of − 1 to + 1 $V_{Ag/AgCl}$. The voltammograms obtained in the second and third scan appear overlapped, proving that the system has reached a steady behavior.

Some of the redox processes that can take place in an aqueous electrolyte composed of antimony and hydrochloric acid are the following [16,17]:

$$Sb^{5+} + 2e^- \leftrightarrows Sb^{3+} \quad (1)$$

$$Sb^{3+} + 3e^- \leftrightarrows Sb^0 \quad (2)$$

$$2Cl^- \leftrightarrows Cl_2 + 2e^- \quad (3)$$

$$2H^+ + 2e^- \leftrightarrows H_2 \quad (4)$$

$$2H_2O \leftrightarrows O_2 + 4H^+ + 4e^- \quad (5)$$

If the voltammograms in Fig. 2 are analyzed from the OCP in the cathodic direction, two reduction peaks can be seen: peak C1, at − 0.39 $V_{Ag/AgCl}$, and peak C2, at − 0.63 $V_{Ag/AgCl}$. Peak C1 corresponds to the reduction of the Sb(III) present in the electrolyte into metallic Sb at the surface of the working electrode (Eq. (2)). Its corresponding oxidation peak (peak A1) is located at − 0.17 $V_{Ag/AgCl}$, which is related to the stripping of the previously deposited Sb. The potential of peak C1 is similar to the reduction potential of Sb(III)/Sb reported in previous studies [18,19]. Majidzade et al. [18] noted that the electrodeposition of antimony in a 0.05 M SbOCl and 0.007 M $C_4H_6O_6$ solution using a Pt electrode began at − 0.44 $V_{Ag/AgCl}$. Sebez et al. [19] observed the reduction of Sb(III) into metallic Sb at − 0.4 $V_{Ag/AgCl}$ with a glassy carbon electrode using 0.01 M HNO_3 and 0.4 mM Sb(III). Peak C2 is related to the adsorption of intermediates of the hydrogen evolution reaction (HER) at the electrode surface. A peak similar to C2, has also been observed by Dubouis and Grimaud [20] at potentials between − 0.13 and + 0.17 $V_{Ag/AgCl}$ with a 0.5 M H_2SO_4 electrolyte; they related this peak to the discharge of protons at the Pt surface. As seen in Fig. 2, at more cathodic potentials than peak C2, the HER takes place (Eq. (4)).

In the anodic scan, apart from peak A1, another oxidation peak can be observed at + 0.75 $V_{Ag/AgCl}$ (peak A3), which corresponds to the oxidation of Sb(III) to Sb(V) (Eq. (1)). Its corresponding reduction peak is C3, which appears at approximately + 0.5 $V_{Ag/AgCl}$ (see inset of Fig. 2). Catrangiu et al. [21] also observed a second redox couple in Sb solutions located near + 0.8 $V_{Ag/AgCl}$ and related it to the Sb(III)/Sb(V) reaction. Yang and Wu [16] detected the potential of the Sb(III)/Sb(V) oxidation process at + 0.35 $V_{Ag/AgCl}$. The variations in the potential values observed for this process can be a consequence of the different electrolytes employed in each work. It is important to note that peak C3 is not visible in the first scan because the cyclic voltammogram began at + 0.59 $V_{Ag/AgCl}$ (OCP). It is necessary that the oxidation of Sb(III)/Sb(V) takes place in peak A3 of the previous scan to observe peak C3 afterwards.

The chloride to chlorine oxidation (Eq. (3)) is located at potentials higher than + 0.9 $V_{Ag/AgCl}$ and its corresponding cathodic reduction peak is placed at about + 0.91 $V_{Ag/AgCl}$ (peak C4). These values of potential are similar to those attributed by other authors to the chlorine reduction; García-Gabaldón et al. detected the reduction of chlorine gas at almost the same potential, + 0.9 $V_{Ag/AgCl}$ [22].

The effect of HCl concentration on the electrochemical behavior of the system is presented in Fig. 3. Two different concentrations of HCl have been tested, 1.5 and 6 M. Hydrochloric acid concentrations lower than 1.5 M could not be used because of the precipitation of Sb(III)

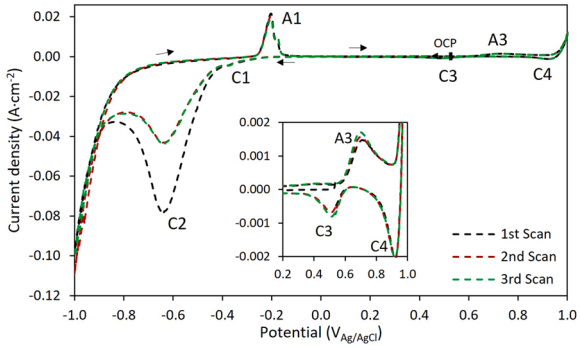

Fig. 2. Cyclic voltammograms obtained with 2 mM Sb and 6 M HCl using the static cell. Scan rate: 10 mV s^{-1}. Working electrode: Pt. Inset: Zoom of peaks A3, C3 and C4.

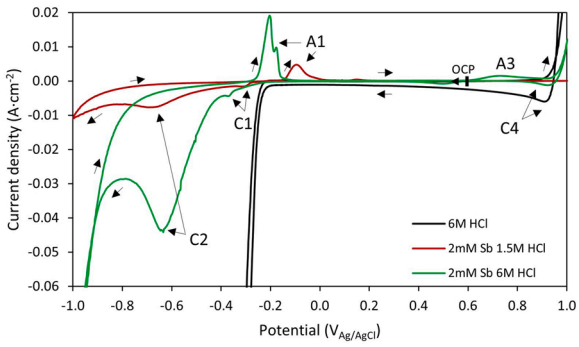

Fig. 3. Cyclic voltammograms obtained with 6 M HCl solutions, mixtures of 6 M HCl and 2 mM Sb; and mixtures of 1.5 M HCl and 2 mM Sb using the static cell. Scan rate: 10 mV s^{-1}. Working electrode: Pt.

oxychlorides. Hashimoto et al. [23] also observed this phenomenon when they studied the hydrolysis of Sb(III) in hydrochloric acid solutions.

If the voltammogram of HCl in the absence of Sb is analyzed, it can be seen that the HER (Eq. 4) begins at − 0.2 $V_{Ag/AgCl}$. With the presence of Sb in the electrolyte, peaks C1 and A1, associated with Sb(III)/Sb, and peak C2, associated with the adsorption of HER intermediates, can be observed. Peak A3, corresponding to the oxidation of Sb(III) to Sb(V), cannot be seen in 1.5 M HCl, whereas it is clearly visible in 6 M HCl. These findings are in agreement with the ones of Kiekens et al. [24] that reported an increase in the redox current for Sb(V) with higher hydrochloric acid concentrations. In addition, it can be observed that Sb inhibits the HER, which appears at about − 0.2 $V_{Ag/AgCl}$ in the absence of Sb and at more cathodic potentials when the reaction happens over the previously deposited Sb. Other authors have also reported this phenomenon; Del Frari et al. [25] concluded that antimony may act as a catalytic poison, causing an overvoltage for the HER. Peak C4, associated with the reduction of chlorine formed during the oxidation scan, increases with the HCl concentration.

Following with the effects of HCl on the deposition of Sb, it can be noted that the current of peaks C1 and A1, attributed to the Sb(III)/Sb redox process, increases with the HCl concentration. Therefore, it can be concluded that an increase in HCl concentration improves the Sb deposition.

In order to understand the electrochemical reactions taking place in the emulated effluent, the distribution of Sb(III) complexes in a chloride solution has been obtained. Senanayake and Muir [26] discussed the speciation of Sb(III) in chloride solutions, concluding that, in a chloride solution at pH < 1, Sb(III) is mainly in the form of chlorocomplexes. The solution studied in this work presents a pH value lower than zero, due to the high hydrochloric acid concentration, so that the main species of Sb (III) present in the solution are chlorocomplexes. In chloride media, the antimony complexes that can be formed are $SbCl^{2+}$, $SbCl_2^+$, $SbCl_3$, $SbCl_4^-$, $SbCl_5^{2-}$ and $SbCl_6^{3-}$. The equilibrium constants and their corresponding reactions are presented below [27]:

$$Sb^{3+} + Cl^- \leftrightarrows SbCl^{2+} \qquad \log\beta_1 = 2.26 \tag{6}$$

$$Sb^{3+} + 2Cl^- \leftrightarrows SbCl_2^+ \qquad \log\beta_2 = 3.49 \tag{7}$$

$$Sb^{3+} + 3Cl^- \leftrightarrows SbCl_3 \qquad \log\beta_3 = 4.18 \tag{8}$$

$$Sb^{3+} + 4Cl^- \leftrightarrows SbCl_4^- \qquad \log\beta_4 = 4.72 \tag{9}$$

$$Sb^{3+} + 5Cl^- \leftrightarrows SbCl_5^{2-} \qquad \log\beta_5 = 4.72 \tag{10}$$

$$Sb^{3+} + 6Cl^- \leftrightarrows SbCl_6^{3-} \qquad \log\beta_6 = 4.11 \tag{11}$$

The speciation diagram of Sb(III) in hydrochloric acid solutions as a function of pCl was obtained (Fig. S.1, Supplementary material). As can be seen, for pCl < 0, all Sb present in the bath is in the form of chorocomplexes. Both hydrochloric acid concentrations employed have been marked. Identifying the predominant complex specie as a function of the HCl concentration may help us to explain the absence or presence of peak A3. For 1.5 M HCl the main specie is $SbCl_5^{2-}$, and for 6 M HCl, $SbCl_6^{3-}$. Hence, peak A3 could be associated with a reaction involving $SbCl_6^{3-}$.

To verify the correlation between peak C1 and the electrodeposition of Sb, the cathodic inversion potential was varied (see Fig. 4). In these experiments, the inversion potentials were − 0.4, − 0.6, − 0.8 and − 1 $V_{Ag/AgCl}$. If the scan is reversed at potentials less cathodic than − 0.4 $V_{Ag/AgCl}$, no oxidation peak is observed. This fact confirms that the Sb(III) reduction begins at potentials near − 0.4 $V_{Ag/AgCl}$, in peak C1. In the reverse scan, the current of the dissolution peak of Sb (peak A1) increases as a function of the inversion potential, that is, as the amount of deposited Sb increases. The potential of peak A1 is independent of the inversion potential, which means that there is no change in the deposit composition.

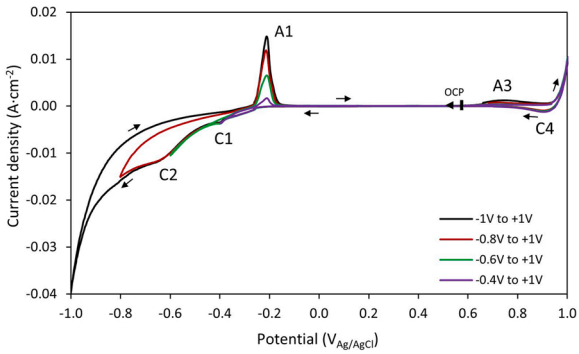

Fig. 4. Cyclic voltammograms obtained at various cathodic inversion potentials with solutions of 2 mM Sb and 6 M HCl using the static cell. Scan rate: 10 mV s^{-1}. Working electrode: Pt.

A cyclic voltammetric study with different concentrations of antimony was carried out to verify the hypothesis presented about the peaks observed in Fig. 2. In Fig. 5, the effect of the Sb concentration on the shape of the voltammograms can be observed. Regarding peak C1, the peak current rises with the increase of Sb concentration, which corroborates that C1 is related to Sb deposition. Furthermore, the potential of peak C1 is shifted towards less cathodic potentials (Fig. 5 inset), which means that the deposition of Sb(III) ions is facilitated by increasing their concentration in solution. A similar behavior was observed by Majidzade et al. [18] at concentrations of SbOCl between 5 and 7 mM in a solution of 7 mM $C_4H_6O_6$. Regarding peak C2, related to the adsorption of HER intermediates at the electrode surface, its current density decreases at increasing Sb concentrations (Fig. 5). According to these results, it can be concluded that Sb acts as an inhibitor of the HER.

In Fig. 5 it can also be observed that an increase in the Sb concentration causes the detection of a shoulder in peak A1. Various authors have tried to explain this phenomenon. Sebez et al. [19] observed a second peak at − 0.008 $V_{Ag/AgCl}$ following the main oxidation peak in consecutive cyclic voltammograms, which was named reoxidation peak and was attributed to Sb-hydroxides/oxides that could be formed at anodic potentials. The newly formed species may not dissolve, thus remaining adsorbed on the electrode surface. Metikoš-Huković et al. [28] also observed multi oxidation peaks at − 0.068 $V_{Ag/AgCl}$ and interpreted them as the nucleation and growth of Sb hydroxide/oxide layers. Wang and Wang [29] reported that the oxidation peak split into two peaks. The first one, placed at more negative potentials (− 0.85 $V_{Ag/AgCl}$) represented the oxidation of the Sb metal on Sb substrate, and the second one, at − 0.75 $V_{Ag/AgCl}$, the oxidation of the first Sb layers electrodeposited on the electrode surface.

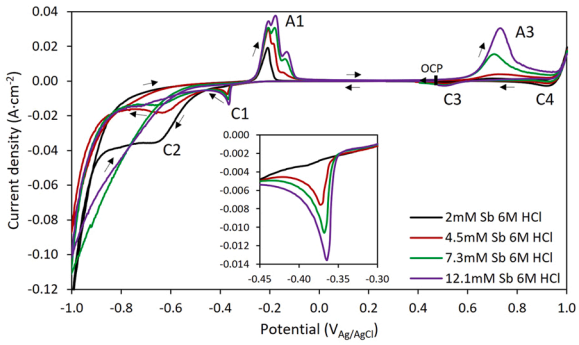

Fig. 5. Cyclic voltammograms obtained for various antimony concentrations and 6 M HCl using the static cell. Scan rate: 10 mV s^{-1}. Working electrode: Pt. Inset: Zoom of peak C1.

At potentials more anodic than A1, peak A3 associated with the oxidation of Sb(III) to Sb(V) becomes larger with an increase in the Sb (III) concentration. The same behavior is observed in its corresponding reduction peak C3. According to the work of Kiekens et al. [24], the predominant chlorocomplex specie of Sb(V) in 6 M HCl solutions is $SbCl_6^-$; therefore, the redox process associated with peaks A3 and C3 may be represented by the following reaction:

$$SbCl_6^{3-} \leftrightarrows SbCl_6^- + 2e^- \quad (12)$$

To further characterize the electrochemical behavior of the Sb(III)/Sb system, which is the reaction of interest for the electrodeposition experiments, the influence of the scan rate on the voltammograms of a 20 mM Sb(III) solution is presented in Fig. 6. It can be seen that the potential of the cathodic peak C1 shifts to more negative values and its peak current increases with an increase in the scan rate. Regarding the effect of the scan rate on the oxidation peak A1, at the lower scan rates of 10–40 mV s^{-1}, a single peak located at − 0.1 $V_{Ag/AgCl}$ is observed, being the peak potential and current independent of the scan rate. Probably, this fact is related to the formation of Sb-hydroxides/oxides mentioned before. By increasing the scan rate, peak A1 is split into two peaks, where the maximum current density of the left part increases, and that of the right part decreases. As the scan rate increases, the oxidation of the deposited Sb and its diffusion within the solution is faster, thus impeding the formation of other compounds such as Sb-hydroxides/oxides. Additionally, the increasing current density of peak A1 reveals that, at higher scan rates, a thicker Sb deposit is formed, which then requires longer times in the anodic scan to get dissolved. The relatively large potential difference between the reduction and the oxidation peaks ($\Delta E_p = E_{pa} - E_{pc}$), larger than 59/n mV, indicates a poor electrochemical reversibility of the Sb(III)/Sb system. Sebez et al. [19] highlighted the weak reversibility of the redox couple in a 0.4 mM Sb (III) and 0.01 M HNO_3 mixture due to the significant potential difference between the reduction and oxidation peaks.

According to the Langmuir isothermal adsorption theory, if ion adsorption is involved in the electrochemical reaction, the relationship between i_p and scan rate, ν, is linear. On the contrary, i_p changes linearly with the square root of scan rate, $\nu^{1/2}$, if the current peak is caused only by ion diffusion [30]. The relationships between i_p and ν as well as between i_p and $\nu^{1/2}$ for peak C1 have been represented in Fig. 6b. Among both types of representation, the relationship between the peak current density and the square root of the scan rate is the one which better fits into a linear regression, indicating that the Sb reduction reaction is controlled by diffusion. The reduction process of Sb(III) into metallic Sb has been reported by several authors to be mass transfer-controlled. Wei et al. [31] also obtained a linear relationship between i_p and $\nu^{1/2}$, confirming that the electrodeposition of Sb(III) is controlled by mass transfer. Thus, the Randles-Ševčík expression modified for irreversible systems at 298 K (Eq. (13)) can be applied [32]:

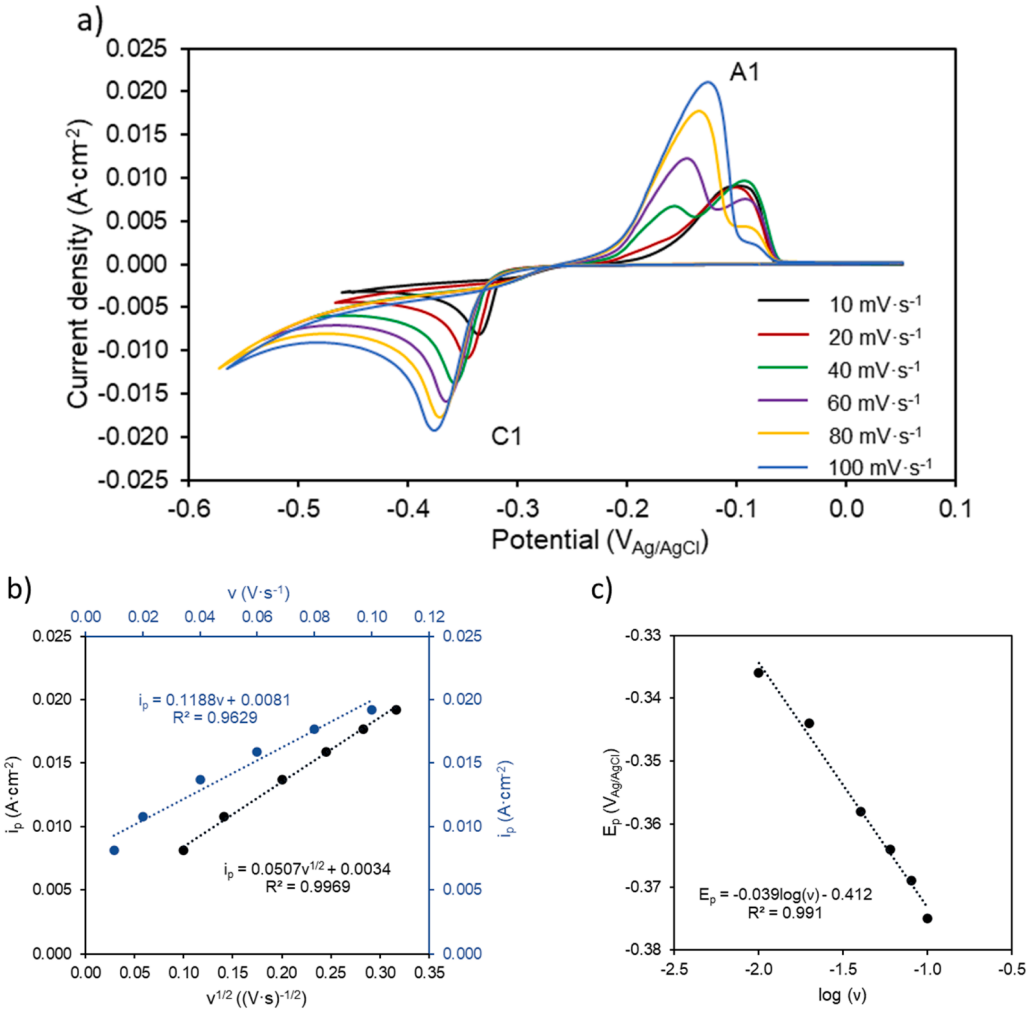

Fig. 6. a) Cyclic voltammograms obtained with 20 mM Sb and 6 M HCl using the static cell at various scan rates. Working electrode: Pt. b) Variation of peak C1 current density as a function of the square root of the scan rate and as a function of the scan rate. c) Variation of peak C1 potential as a function of the logarithm of the scan rate.

$$i_p = 2.99 \cdot 10^5 \cdot n \cdot (\alpha \cdot n_\alpha)^{\frac{1}{2}} \cdot D^{\frac{1}{2}} \cdot C_0 \cdot \nu^{\frac{1}{2}} \quad (13)$$

where α is the transfer coefficient; n_α is the number of electrons involved in the rate-determining step; D is the diffusion coefficient, $cm^2\ s^{-1}$; C_0 is the bulk concentration, mol cm^{-3}; and ν corresponds to the value of the scan rate, V s^{-1}. The value of $\alpha \cdot n_\alpha$ has been estimated from the expression deduced by Laviron for cathodic peaks, applied to redox systems with $\Delta E_p > 200/n$ mV [33]. As indicated by Laviron, this value has been obtained from the semilogarithmic representation of the cathodic peak potential versus the scan rate (Fig. 6c), where the resulting straight line has a slope of $-2.3 \cdot R \cdot T/\alpha \cdot n_\alpha$. According to Eq. (13) and the slope obtained from Fig. 6b, the diffusion coefficient related to the Sb deposition, peak C1, is $5.27 \cdot 10^{-6}$ $cm^2\ s^{-1}$. This value is of the same order of magnitude as those obtained by other authors: the diffusion coefficient of Sb (III) electrodeposition in alkaline solutions containing xylitol calculated by Liu et al. [34] was $1.53 \cdot 10^{-6}$ $cm^2\ s^{-1}$.

3.2. Electrochemical study using the RDE cell

In order to better understand the kinetics of antimony electrodeposition, a set of linear voltammograms was measured on a Pt RDE at rotation rates ranging from 500 to 4500 rpm. Fig. 7 presents the linear voltammograms obtained in the potential range from 0 to − 0.6 $V_{Ag/AgCl}$ at a scan rate of 10 mV s^{-1}. Similar to the results obtained with the static cell already shown in Fig. 4, deposition of Sb(III) took place only when potential values more cathodic than − 0.32 $V_{Ag/AgCl}$ were reached. Between − 0.4 and − 0.5 $V_{Ag/AgCl}$, approximately, a plateau related to a limiting current density is obtained, indicating that the Sb(III) reduction is under complete mass transfer-control. As can be seen in Fig. 7, the limiting current density increases with the electrode rotation rate.

The inset of Fig. 7 represents the relationship between the current density and the square root of the rotation rate for the plateau current density. These values present a linear dependence, which is typical of diffusion-controlled processes, in agreement with the Levich theory for rotating disk electrodes. Accordingly, the Levich equation (Eq. (14)) [35] was applied to obtain the diffusion coefficient (D):

$$i_L = 0.621 \cdot n \cdot F \cdot D^{2/3} \cdot \nu^{-1/6} \cdot C_0 \cdot \omega^{1/2} \quad (14)$$

In Eq. (14), F corresponds to the Faraday constant, 96,485.33 C mol^{-1}; ν is the solution kinematic viscosity, 0.013 $cm^2\ s^{-1}$ for a solution containing 6 M HCl at 25 °C [36]; and ω is the rotation rate, rad s^{-1}. The diffusion coefficient calculated using this equation is $5.31 \cdot 10^{-6}$ $cm^2\ s^{-1}$, which is very similar to the value calculated from the Randles- Ševčík equation (Eq. (13)). Previous to the electrodeposition experiments, linear voltammetric scans were conducted in the RDE cell also using a copper electrode, to evaluate the influence of the electrode material on the electrochemical behavior of the Sb-HCl

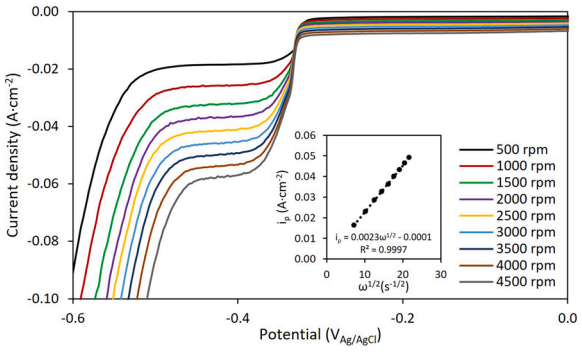

Fig. 7. Linear sweep voltammograms obtained with 20 mM Sb and 6 M HCl solutions using the RDE at various rotation rates. Scan rate: 10 mV s^{-1}. Working electrode: Pt. Inset: Relationship between limiting current density and the square root of the rotation speed.

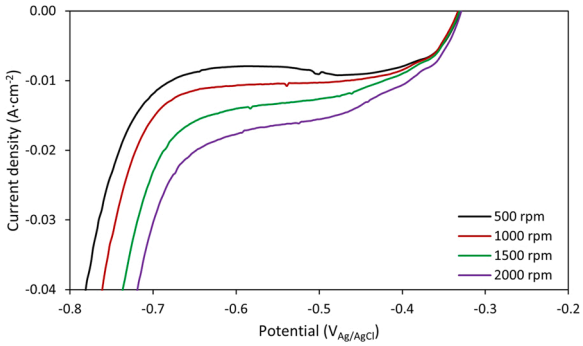

Fig. 8. Linear sweep voltammograms obtained with 2 mM Sb and 6 M HCl solutions using the RDE cell at various rotation rates. Scan rate: 10 mV s^{-1}. Working electrode: Cu.

system. Fig. 8 shows the voltammograms obtained with copper electrodes. The deposition of Sb(III) starts at approximately − 0.33 $V_{Ag/AgCl}$. The linear voltammograms include a plateau related to the limiting current density of the Sb(III) reduction, which was also observed with the platinum electrode (Fig. 7). The plateau obtained with the copper electrode appears between − 0.40 and − 0.60 $V_{Ag/AgCl}$. With the platinum electrode, the plateau begins near − 0.40 and ends at − 0.50 $V_{Ag/AgCl}$. In both cases, the plateau has a similar shape and corresponds to the bulk deposition of antimony.

The reduction potentials of antimony in both materials, copper and platinum, are very similar. Therefore, subsequent antimony electrodeposition experiments were conducted on copper disk electrodes. Copper was selected as a suitable electrode material to minimize the cost of electrodeposition of Sb in the copper industry. Furthermore, the efficiency of copper as cathode for the electrodeposition of Sb has been highlighted in several studies. Bergmann and Koparal [8] studied various cathodic materials for the electrochemical deposition of Sb in H_2SO_4 solutions, and concluded that copper is one of the best materials for such purpose.

3.3. Electrodeposition experiments

As mentioned in Section 2.3, electrodeposition experiments were carried out in potentiostatic and galvanostatic mode using both the static and the RDE cell. The surface and elemental analysis of the deposits obtained using the static cell under potentiostatic conditions are shown in Fig. 9. The SEM image of the deposit obtained at − 0.40 $V_{Ag/AgCl}$ (Fig. 9a) shows a homogeneous coating and some dispersed globular grains of variable size, approximately between 250 and 1250 nm. This value of applied potential corresponds to the beginning of the Sb(III)/Sb electrodeposition process, as observed in the previous voltammograms. When a more cathodic electrode potential of − 0.50 $V_{Ag/AgCl}$ is applied (Fig. 9b), the electrode surface becomes covered with grains of metallic antimony of a size varying between 100 and 200 nm. In addition to this, the growth of dendrites of variable size predominates over the granular surface. By comparing Fig. 9a with Fig. 9b, it can be seen that an increase in potential from − 0.40 to − 0.50 $V_{Ag/AgCl}$ involves a decrease in the grain diameter. This behavior can be explained by an increased nucleation rate when higher values of potential are applied. As a consequence, the deposition starts to take place predominantly in the form of dendrites instead of granules.

When the applied potential becomes even more cathodic, reaching values of − 0.65 and − 0.80 $V_{Ag/AgCl}$ (see Fig. 9c and d), the grain surface, also observed for the other potentials, becomes covered by powder-like deposits. At the highest potential, the deposits turn more porous and show a low adherence to the substrate. These highly cathodic potentials, − 0.65 and − 0.80 $V_{Ag/AgCl}$, correspond to the region in the voltammograms where the HER becomes relevant. Consequently, the intense HER impedes the homogeneous growth of metallic Sb and causes deposit

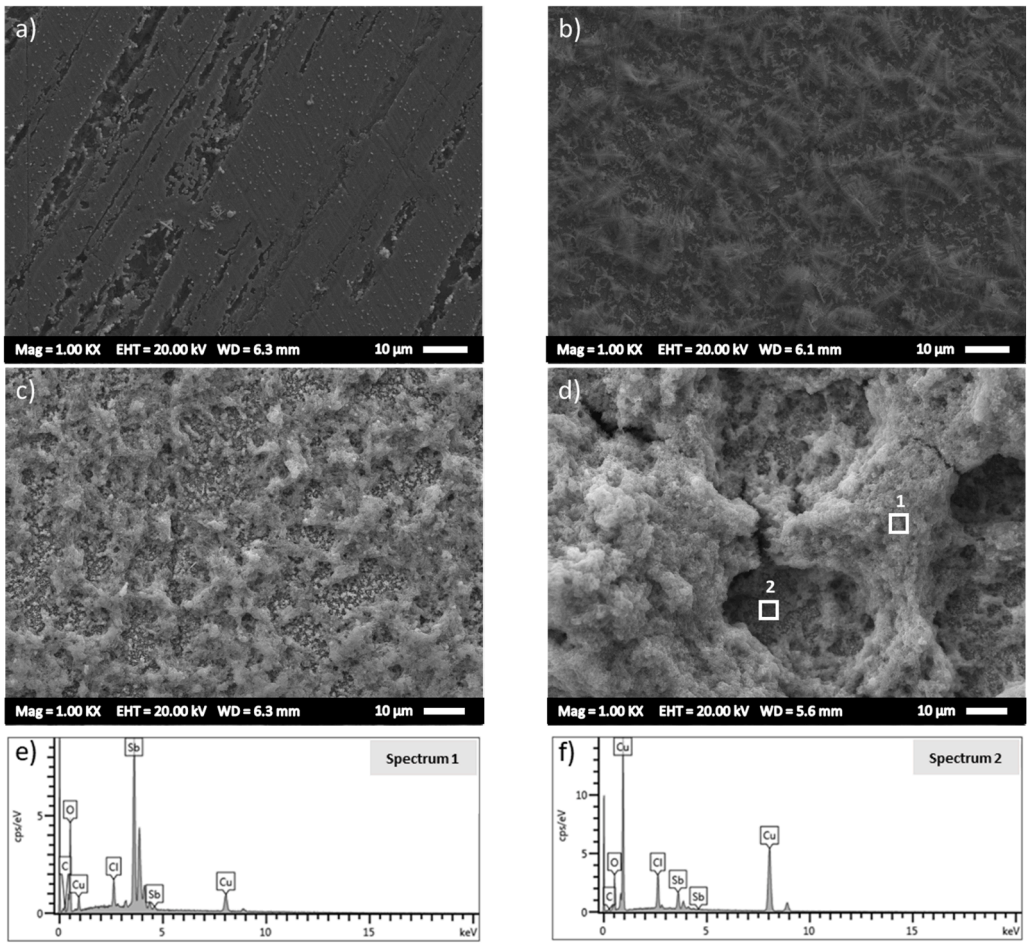

Fig. 9. SEM images of the deposits obtained in potentiostatic mode on copper electrode during 30 min with 2 mM Sb and 6 M HCl using the static cell: a) − 0.40 $V_{Ag/AgCl}$; b) − 0.50 $V_{Ag/AgCl}$; c) − 0.65 $V_{Ag/AgCl}$; d) − 0.80 $V_{Ag/AgCl}$. EDX spectra of the deposit obtained at − 0.80 $V_{Ag/AgCl}$: e) Zone 1; f) Zone 2.

erosion, giving place to highly porous structures.

Fig. 9e and f show the EDX spectra obtained at two different locations marked in Fig. 9d (zone 1 and zone 2 of the electrode surface). As it can be seen, in regions where the electrodeposition dominates (zone 1), that is, at the edges of the pores, a big peak associated with Sb was obtained in the spectrum (Fig. 9e). However, in zone 2, where the formation of hydrogen bubbles was vigorous, the deposition of metallic Sb was hampered and the substrate electrode material, Cu, is the predominant element detected (Fig. 9f).

When the deposition using the static cell is controlled galvanostatically, the morphologies obtained at a given current density are very similar to those previously obtained in potentiostatic mode at the corresponding potentials. Fig. 10 shows the SEM images of the deposits obtained with the static cell at two levels of constant current density. Under the application of a current density of $-4.40 \cdot 10^{-4}$ A cm^{-2} (Fig. 10a), dispersive and circular grains, with their size varying between 500 and 700 nm, grow over a homogeneous coating surface. This morphology is very similar to that obtained in potentiostatic mode at − 0.4 $V_{Ag/AgCl}$, where an average current density of $-4.36 \cdot 10^{-4}$ A cm^{-2} was registered during the electrodeposition tests (Table S. 1, Supplementary material).

If a higher current density of − 0.001 A · cm^{-2} is applied (Fig. 10b),

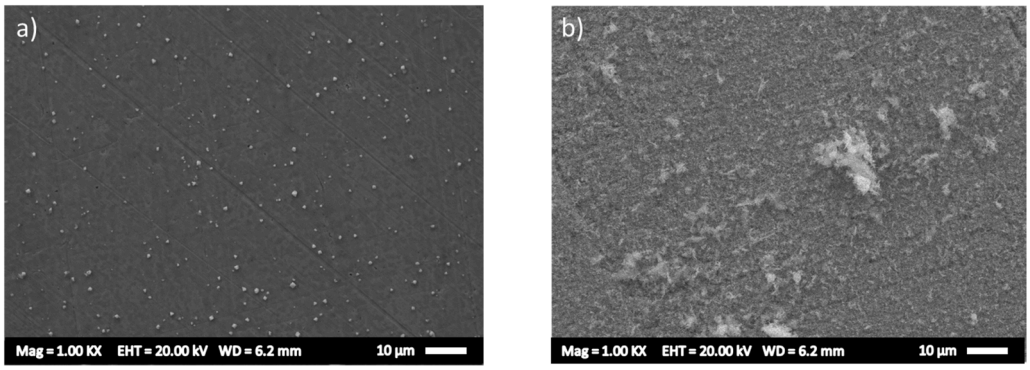

Fig. 10. SEM images of the deposits obtained in galvanostatic mode on copper electrode during 30 min with 2 mM Sb and 6 M HCl using the static cell: a) $-4.40 \cdot 10^{-4}$ A cm^{-2}; b) − 0.001 A · cm^{-2}.

the electrode surface becomes also covered by circular grains, in this case of a size between 300 and 400 nm. As occurred in the potentiostatic tests when the operation was shifted towards more cathodic conditions, an increase in current density in the galvanostatic operation also involves higher deposition rates and leads to smaller grain sizes. A strong correlation can be found with the potentiostatic electrodeposition conducted at $-0.50\ V_{Ag/AgCl}$, where an average current density of $-7 \cdot 10^{-4}$ A cm^{-2} was registered during the tests. In this case, a shift towards more cathodic conditions also involves the formation of dendrites. In summary, it can be concluded that the morphology of the Sb deposits obtained in the galvanostatic tests without stirring is analogous to that obtained in the potentiostatic tests in which a similar average current density was registered.

As confirmed in the voltammetric study conducted with the RDE (Section 3.2), the process of Sb electrodeposition is controlled by the supply of dissolved antimony to the electrode surface, so that higher deposition rates may be expected under intensified hydrodynamic conditions. This was tested by conducting further electrodeposition tests with the RDE under potentiostatic and galvanostatic conditions. The potential values for the potentiostatic tests were selected to comprise the plateau region of the voltammograms registered at 1500 rpm (Fig. 8): -0.40 and $-0.65\ V_{Ag/AgCl}$ (here it is to note that the length of the plateau region becomes shorter with an increase of the rotating rate). The SEM images of these experiments are presented in Fig. 11. At $-0.40\ V_{Ag/AgCl}$ (Fig. 11a), the electrode surface appears covered by grains of irregular shape, including needles and dendrites of variable size. Over this heterogenous layer, the growth of dendrites with a length of up to 10 μm predominates. At an applied potential of $-0.65\ V_{Ag/AgCl}$, the electrodeposition rate increases (the average current density of this test is higher than at $-0.40\ V_{Ag/AgCl}$, see Table S. 2 of the Supplementary material); and the deposit turns into powder agglomerates. Furthermore, the growth of the deposit is irregular due to the generation of hydrogen bubbles. The predominance of the HER is more visible at the highest applied potential because this value corresponds to the end of the plateau for this stirring rate (Fig. 8).

The current densities applied in the galvanostatic experiments with the RDE cell were selected taking as a reference the limiting current density registered in the voltammogram obtained with the RDE at 1500 rpm ($i_L = 0.0147$ A cm^{-2}, see Fig. 8). The experiments were carried out slightly below (-0.0125 A cm^{-2}) and at a current density significantly exceeding this value (-0.075 A cm^{-2}).

Fig. 12 shows the SEM images of the deposits obtained in galvanostatic mode using the RDE cell. The deposit obtained at -0.0125 A cm^{-2} presents a mixed morphology between dendritic and a powder-like shape. Although the applied current density is below the corresponding i_L, the enhanced hydrodynamic conditions improve the supply of dissolved antimony to the electrode surface, thus involving a higher nucleation rate and the consequent formation of dendrites within the 30 min of electrodeposition tests. If the current density is increased up to -0.075 A cm^{-2}, the obtained deposit becomes entirely porous and brittle, as a consequence of the intense HER. The wheat-like grains resulting at -0.0125 A cm^{-2} (Fig. 12a) were also observed by Bu et al. [37] using choline chloride-ethylene glycol as electrolyte in a titanium electrode. As commented above for the static cell, the morphology of the deposits obtained in galvanostatic mode is very similar to that obtained in potentiostatic tests. The reason for this is that the applied current densities are very similar to the average ones measured during the potentiostatic experiments (see Table S. 2, Supplementary material).

In Fig. 8 it was observed that the limiting current density increases at higher rotation rates as a consequence of an enhanced electrodeposition rate. The improved mass transfer caused by the stirring was also confirmed in the electrodeposition tests, since higher current densities were reached for the same electrodeposition potential when the system was stirred (the average current density was $-4.36 \cdot 10^{-4}$ A cm^{-2} at $-0.4\ V_{Ag/AgCl}$ under static conditions, whereas it reached the value of -0.0125 A cm^{-2} at the same potential under hydrodynamic conditions, see Table S. 1, Supplementary material). Although stirring implies higher deposition rates, exceeding the limiting current density might also imply the formation of porous and weak deposits (Fig. 12b).

4. Conclusions

In the present work, an electrochemical study was conducted to evaluate the recovery of antimony by means of electrodeposition from highly concentrated HCl solutions generated in the copper electrorefining. Voltammetric curves allowed us to identify the current density and potential values at which the redox processes of Sb(III)/Sb, Sb(V)/Sb(III), Cl_2/Cl^-, and HER occur. Even though the high concentration of acid in the electrolyte implies the occurrence of the HER, our results prove that Sb deposition improves at high HCl concentrations. Thus, it can be concluded that metallic Sb acts as a partial inhibitor of the HER. Cyclic voltammetry tests at various scan rates and at different rotation rates demonstrated that Sb deposition is a mass transfer-controlled process. The average diffusion coefficient of Sb estimated from the Randles- Ševčík and Levich equations was $5.29 \pm 0.20 \cdot 10^{-6}$ cm^2 s^{-1}.

The Sb(III) deposition starts at $-0.4\ V_{Ag/AgCl}$, as observed in the voltammograms and corroborated in the electrodeposition tests by means of SEM and EDX. Sb was detected at the surface of the copper electrode after 30 min of electrodeposition at potentials more cathodic than $-0.4\ V_{Ag/AgCl}$, both under static and stirring conditions. In potentiostatic mode, the deposits obtained using the static cell at potentials less cathodic than $-0.65\ V_{Ag/AgCl}$ were very adherent to the electrode surface. At more cathodic potentials, the deposits were not so adherent and suffered erosion. The use of the RDE cell is a key factor in reducing mass transfer limitations, leading to a significant increase in current density and to a faster recovery of antimony. Similar conclusions can be extracted from the galvanostatic tests: the deposits obtained at the highest current densities (in absolute value) are less compact and

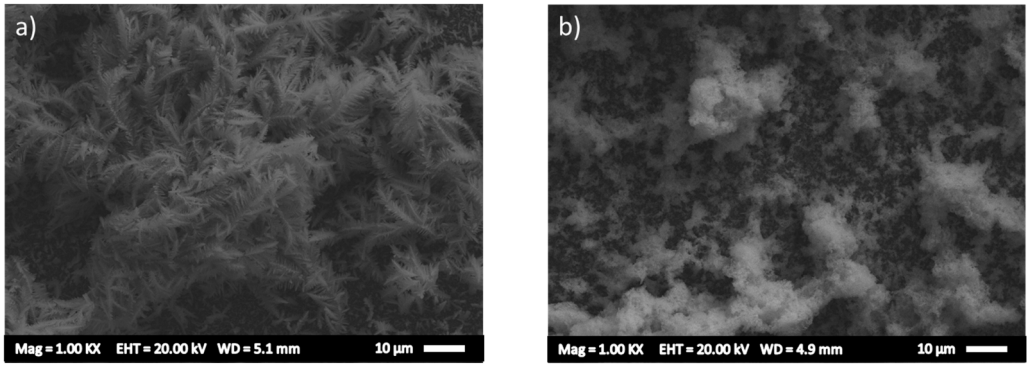

Fig. 11. SEM images of the deposits obtained in potentiostatic mode on copper electrode during 30 min with 2 mM Sb and 6 M HCl using the RDE cell: a) $-0.40\ V_{Ag/AgCl}$; b) $-0.65\ V_{Ag/AgCl}$.

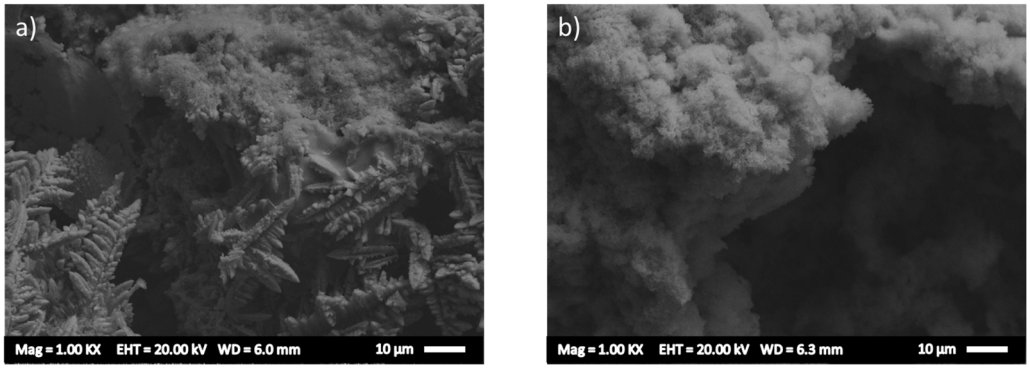

Fig. 12. SEM images of the deposits obtained in galvanostatic mode on copper electrode during 30 min with 2 mM Sb and 6 M HCl using the RDE cell: a) − 0.0125 A cm^{-2}; b) − 0.075 A cm^{-2}.

more fragile. In general, most of the deposits present dendritic growth and porous shape because the HER is more relevant as the values of applied potential and current density become more cathodic.

CRediT authorship contribution statement

L. Hernández-Pérez: Investigation, Writing – original draft, Visualization. **J. Carrillo-Abad:** Methodology, Validation. **E.M. Ortega:** Investigation. **V. Pérez-Herranz:** Project administration, Funding acquisition, Writing – review & editing. **M.T. Montañés:** Conceptualization, Supervision, Writing – review & editing. **M.C. Martí-Calatayud:** Conceptualization, Supervision, Writing – review & editing.

Declaration of Competing Interest

The authors declare that they have no known competing financial interests or personal relationships that could have appeared to influence the work reported in this paper.

Data Availability

Data will be made available on request.

Acknowledgments

The authors thank the financial support from the Agencia Estatal de Investigación (AEI/10.13039/501100011033) (Spain) under the project PCI2019-103535 and by FEDER A way of making Europe. Funding for open access charge: CRUE-Universitat Politècnica de València.

Appendix A. Supporting information

Supplementary data associated with this article can be found in the online version at doi:10.1016/j.jece.2022.109139.

References

[1] European Commission, Communication from the Commission to the European Parliament, the Council, the European Economic and Social Committee and the Committee of the Regions: tackling the challenges in commodity markets and on raw materials, Brussels, 2011.
[2] G. Ungureanu, S.C.R. Santos, I. Volf, R.A.R. Boaventura, C.M.S. Botelho, Biosorption of antimony oxyanions by brown seaweeds: batch and column studies, J. Environ. Chem. Eng. 5 (2017) 3463–3471, https://doi.org/10.1016/J.JECE.2017.07.005.
[3] H. Ling, B. Blanpain, M. Guo, A. Malfliet, Characterization of antimony-containing metallurgical residues for antimony recovery, J. Clean. Prod. 327 (2021), 129491, https://doi.org/10.1016/J.JCLEPRO.2021.129491.
[4] D. Dupont, S. Arnout, P.T. Jones, K. Binnemans, Antimony recovery from end-of-life products and industrial process residues: a critical review, J. Sustain. Met. 2 (2016) 79–103, https://doi.org/10.1007/s40831-016-0043-y.
[5] P. Navarro, F.J. Alguacil, Adsorption of antimony and arsenic from a copper electrorefining solution onto activated carbon, Hydrometallurgy 66 (2002) 101–105, https://doi.org/10.1016/S0304-386X(02)00108-1.
[6] H. Cao, J. Chen, H. Yuan, G. Zheng, Preparation of pure $SbCl_3$ from lead anode slime bearing high antimony and low silver, Trans. Nonferrous Met. Soc. China (Engl. Ed.) 20 (2010) 2397–2403, https://doi.org/10.1016/S1003-6326(10)60661-9.
[7] S. Ubaldini, F. Vegliò, P. Fornari, C. Abbruzzese, Process flow-sheet for gold and antimony recovery from stibnite, Hydrometallurgy 57 (2000) 187–199, https://doi.org/10.1016/S0304-386X(00)00107-9.
[8] M.E.H. Bergmann, A.S. Koparal, Electrochemical antimony removal from accumulator acid: results from removal trials in laboratory cells, J. Hazard. Mater. 196 (2011) 59–65, https://doi.org/10.1016/J.JHAZMAT.2011.08.073.
[9] S.S. Koparal, R. Özgür, Ü.B. Öğütveren, H. Bergmann, Antimony removal from model acid solutions by electrodeposition, Sep. Purif. Technol. 37 (2004) 107–116, https://doi.org/10.1016/j.seppur.2003.09.001.
[10] S.A. Awe, K. Sandström, Selective leaching of arsenic and antimony from a tetrahedrite rich complex sulphide concentrate using alkaline sulphide solution, Miner. Eng. 23 (2010) 1227–1236, https://doi.org/10.1016/j.mineng.2010.08.018.
[11] K.S. Barros, V.S. Vielmo, B.G. Moreno, G. Riveros, G. Cifuentes, A.M. Bernardes, Chemical composition data of the main stages of copper production from sulfide minerals in Chile: a review to assist circular economy studies, Minerals 12 (2022), https://doi.org/10.3390/min12020250.
[12] V.R.C. Thanu, M. Jayakumar, Electrochemical recovery of antimony and bismuth from spent electrolytes, Sep. Purif. Technol. 235 (2020), 116169, https://doi.org/10.1016/j.seppur.2019.116169.
[13] L.C. Ward, J.L. Stickney, Electrodeposition of Sb onto the low-index planes of Cu in aqueous chloride solutions: studies by LEED, AES and electrochemistry, Phys. Chem. Chem. Phys. 3 (2001) 3364–3370, https://doi.org/10.1039/b101983j.
[14] H. Cao, Y. Zhong, L. Wu, Y. Zhang, G. Zheng, Electrodeposition of As-Sb alloy from high arsenic-containing solutions, Trans. Nonferrous Met. Soc. China (Engl. Ed.) 26 (2016) 310–318, https://doi.org/10.1016/S1003-6326(16)64120-1.
[15] C. González-Buch, I. Herraiz-Cardona, E. Ortega, J. García-Antón, V. Pérez-Herranz, Study of the catalytic activity of 3D macroporous Ni and NiMo cathodes for hydrogen production by alkaline water electrolysis, J. Appl. Electrochem. 46 (2016) 791–803, https://doi.org/10.1007/s10800-016-0970-0.
[16] J.G. Yang, Y.T. Wu, A hydrometallurgical process for the separation and recovery of antimony, Hydrometallurgy 143 (2014) 68–74, https://doi.org/10.1016/j.hydromet.2014.01.002.
[17] P.A. Riveros, J.E. Dutrizac, R. Lastra, A study of the ion exchange removal of antimony(III) and antimony(V) from copper electrolytes, Can. Metall. Q. 47 (2008) 307–316, https://doi.org/10.1179/cmq.2008.47.3.307.
[18] V.A. Majidzade, P.H. Guliyev, A.S. Aliyev, M. Elrouby, D.B. Tagiyev, Electrochemical characterization and electrode kinetics for antimony electrodeposition from its oxychloride solution in the presence of tartaric acid, J. Mol. Struct. 1136 (2017) 7–13, https://doi.org/10.1016/j.molstruc.2017.01.082.
[19] B. Sebez, B. Ogorevc, S.B. Hocevar, M. Veber, Functioning of antimony film electrode in acid media under cyclic and anodic stripping voltammetry conditions, Anal. Chim. Acta 785 (2013) 43–49, https://doi.org/10.1016/j.aca.2013.04.051.
[20] N. Dubouis, A. Grimaud, The hydrogen evolution reaction: from material to interfacial descriptors, Chem. Sci. 10 (2019) 9165–9181, https://doi.org/10.1039/c9sc03831k.
[21] A.S. Catrangiu, A. Cotârţə, A. Cojocaru, T. Vişan, Diffusion-controlled reduction of Sb^{3+} and Cu^{2+} to metals from ionic liquids containing choline chloride, UPB Sci. Bull. Ser. B Chem. Mater. Sci. 78 (2016) 13–26.
[22] M. García-Gabaldón, J. Carrillo-Abad, E. Ortega-Navarro, V. Pérez-Herranz, Electrochemical study of a simulated spent pickling solution, Int. J. Electrochem. Sci. 6 (2011) 506–519. ⟨www.electrochemsci.org⟩.
[23] H. Hashimoto, T. Nishimura, Y. Umetsu, Hydrolysis of antimony(III)-hydrochloric acid solution at 25 °C, Mater. Trans. 44 (2003) 1624–1629, https://doi.org/10.2320/matertrans.44.1624.

[24] P. Kiekens, H. Verplaetse, E. Temmerman, Electrochemical study of the Sb(V)/Sb (III) couple on a glassy carbon rotating-disk electrode, J. Electroanal. Chem. 113 (1980) 233–238, https://doi.org/10.1016/S0022-0728(80)80024-6.
[25] D. Del Frari, S. Diliberto, N. Stein, C. Boulanger, J.M. Lecuire, Comparative study of the electrochemical preparation of Bi_2Te_3, Sb_2Te_3, and $(Bi_xSb_{1-x})_2Te_3$ films, Thin Solid Films 483 (2005) 44–49, https://doi.org/10.1016/j.tsf.2004.12.015.
[26] G. Senanayake, D.M. Muir, Speciation and reduction potentials of metal ions in concentrated chloride and sulfate solutions relevant to processing base metal sulfides, Metall. Trans. B 19 (1988) 37–45, https://doi.org/10.1007/BF02666488.
[27] B. Lothenbach, M. Ochs, H. Wanner, Y. Mikazu, Thermodynamic date for the speciation and solubility of Pd, Pb, Sn, Sb, Nb and Bi in aqueous solution, 1999.
[28] M. Metikoš-Huković, R. Babić, S. Omanović, Electrochemical kinetics of anodic layer formation and reduction on antimony and antimonial lead, J. Electroanal. Chem. 374 (1994) 199–206, https://doi.org/10.1016/0022-0728(94)03354-4.
[29] Q. Wang, Y. Wang, Fundamental electrochemical behavior of antimony in alkaline solution, J. Sustain. Met. 5 (2019) 606–616, https://doi.org/10.1007/s40831-019-00253-7.
[30] N. Elgrishi, K.J. Rountree, B.D. McCarthy, E.S. Rountree, T.T. Eisenhart, J. L. Dempsey, A practical beginner's guide to cyclic voltammetry, J. Chem. Educ. 95 (2018) 197–206, https://doi.org/10.1021/acs.jchemed.7b00361.
[31] S. Wei, M. Zhang, W. Han, Y. Yan, Y. Xue, M. Zhang, B. Zhang, Electrochemical behavior of antimony and electrodeposition of Mg-Li-Sb alloys from chloride melts, Electrochim. Acta 56 (2011) 4159–4166, https://doi.org/10.1016/j.electacta.2011.01.104.
[32] A.J. Bard, L.R. Faulkner, Electrochemical Methods: Fundamentals and Applications, Second, John Wiley & Sons, Inc., 2001.
[33] E. Laviron, General expression of the linear potential sweep voltammogram in the case of diffusionless electrochemical systems, J. Electroanal. Chem. 101 (1979) 19–28, https://doi.org/10.1016/S0022-0728(79)80075-3.
[34] W. Liu, T. Yang, Q. Zhou, D. Zhang, C. Lei, Electrodeposition of Sb(III) in alkaline solutions containing xylitol, Trans. Nonferrous Met. Soc. China (Engl. Ed.) 22 (2012) 949–957, https://doi.org/10.1016/S1003-6326(11)61269-7.
[35] A.C. Kasper, H.M. Veit, M. García-Gabaldón, V.P. Herranz, Electrochemical study of gold recovery from ammoniacal thiosulfate, simulating the PCBs leaching of mobile phones, Electrochim. Acta 259 (2018) 500–509, https://doi.org/10.1016/j.electacta.2017.10.161.
[36] D.R. Lide, CRC Press Handbook of Chemistry and Physics, 84th ed., 1995.
[37] J. Bu, J. Ru, Z. Wang, Y. Hua, C. Xu, Y. Zhang, Y. Wang, Controllable preparation of antimony powders by electrodeposition in choline chloride-ethylene glycol, Adv. Powder Technol. 30 (2019) 2859–2867, https://doi.org/10.1016/j.apt.2019.06.027.